Advanced Large-Eddy Simulation for lattice Boltzmann methods : the Approximate Deconvolution Model

Orestis Malaspinas[1, a)] and Pierre Sagaut[1, b)]

Institut Jean Le Rond d'Alembert, UMR CNRS 7190, Université Pierre et Marie Curie - Paris 6

4, place Jussieu, case 162, F-75252 Paris cedex 5, France

(Dated: 25 October 2013)

The aim of this paper is to extend the Approximate Deconvolution Model for Large-Eddy simulations to the lattice Boltzmann method. This approach allows to directly act on the velocity distribution function and is based on the intrinsic nonlinearities of the lattice Boltzmann methods. It is not a straightforward extrapolation of classical eddy-viscosity models developed within the Navier–Stokes framework, which exhibits a convective quadratic nonlinearity in the incompressible flow case. A simple implementation is presented, which relies on the implementation of an ad hoc linear filter in any basic Lattice Boltzmann solver. The new model is validated on the turbulent, time developing mixing layer, and a very satisfactory agreement is found with existing direct numerical simulations results. The equivalent Navier-Stokes-type macroscopic model is also discussed.

Keywords: Lattice Boltzmann Method, Turbulence modeling, Approximate deconvolution model, Large Eddy Simulations, Time developing mixing layer

CONTENTS

[a)] Electronic mail: malaspinas@lmm.jussieu.fr

[b)] Electronic mail: pierre.sagaut@upmc.fr

I. INTRODUCTION

The simulation of turbulent flows is of primary importance in many everyday life applications. The wide increase in the range of scales, involved in the motion of such flows, with the Reynolds number forbids their Direct Numerical Simulation (DNS) (where all scales are simultaneously resolved) of many applications of interest because of the limited capabilities of computers. In order to study the behavior of this class of fluid flows it is necessary to reduce the amount of degrees of freedom needed. One way of doing this is by using Large Eddy Simulation (LES) techniques (see Refs. 1–3) such as the seminal Smagorinsky model[4], where the main idea is to resolve only the large scales of motion and to model the small ones. In this way one is able to considerably reduce the amount of degrees of freedom needed to simulate turbulent flows. Due to the nonlinearity of the governing equations of motion, small unresolved scales and large resolved scales are coupled. Therefore, the removal of the smallest scales of turbulence must be compensated by a modification of the governing equations for resolved scales, in order to account for the effect of missing turbulent eddies. This is done in practice by introducing a subgrid closure. The coupling terms directly stem from the nonlinear term in the basic governing equation since it can be defined as the commutation error between nonlinear terms and a linear scale separation operator. Therefore a change in the nonlinear terms should induce a change in the subgrid closure. Within the Navier-Stokes framework, subgrid models have been improved in many ways during the last decades, by accounting for new physical phenomena (e.g. heat transfer 5 or aeroacoustic noise generation6) or developing multiscale/multidomain approaches 7 and 8, but it is worth noting that the vast majority of proposed subgrid closures relies on the eddy viscosity paradigm.

In the lattice Boltzmann community the huge majority of LES techniques is based on "extrapolations" of eddy viscosity models for the Navier–Stokes equations, like the Smagorinsky model (see Refs. 9–17 among others). These models are based on a local modification of the relaxation time in order to modify the viscosity of the fluid. A first remark is that the direct plugging of Navier-Stokes-based eddy viscosity via a change of the relaxation time in BGK-type methods does not guarantee that the features of the non-linear collision term, which does not ex-

hibit the same nonlinear character as the convection term in incompressible Navier-Stokes equations, are taken into account in a fully satisfactory way. A second remark is that Lattice Boltzmann methods can capture different kinds of physics, ranging from incompressible to fully compressible flows, depending on the truncation order of the Hermite polynomial based series expansion of the exponential nonlinear collision term (and therefore on the order of the nonlinear collision term). As a consequence, a general subgrid closure procedure which automatically adapts itself to nonlinear terms should be sought for.

To this end, we propose here to reuse the idea of the Approximate Deconvolution Model (ADM) of Stolz, Adams and Kleiser[18–20] where the macroscopic fields (density, velocity, ...) are approximately recovered by applying an approximate inverse filter operator on the filtered Navier–Stokes equations. This approach, which does not assume any particular feature of the nonlinear terms and the underlying interscale physics, has successfully been applied to both incompressible and compressible flows, including flows with shock waves[21].

In our case, instead of acting on the macroscopic fields, we apply the Approximate Deconvolution operator directly on the filtered distribution function, which is the basis of the Boltzmann equation, as proposed by Sagaut[22]. Thus, instead of relying only on macroscopic modeling of turbulence, one is able to act directly on a more microscopic level, which provides an alternate methodology. Another point is that each filtered lattice Boltzmann model for large-eddy simulations can be associated with a corresponding macroscopic Navier-Stokes-like equations. Since filtering the Lattice Boltzmann governing equation is uniquely defined, it can also represent an interesting way to derive governing equations for Navier-Stokes based large-eddy simulation for compressible flows, since direct filtering of compressible Navier-Stokes equations is known to lead to an infinity of possible set of equations[3].

The organization of this paper is as follows. In Sec. II the ADM is presented and is applied in the LBM framework. The model is then validated on the time dependent mixing layer in Sec. III which is a classical turbulence benchmark. And finally the paper is concluded in Sec. IV.

II. APPROXIMATE DECONVOLUTION MODEL FOR THE LATTICE BOLTZMANN METHOD

In this section, following the paper by Sagaut[22], the approximate deconvolution method for LBM-LES will be presented.

A. The filtered Boltzmann equation

The continuous Boltzmann equation in absence of an external force with a generic collision operator $\Omega(f)$ reads

$$\frac{\mathrm{d}f}{\mathrm{d}t} \equiv \left(\partial_t + \boldsymbol{\xi}\cdot\boldsymbol{\nabla}_{\boldsymbol{x}}\right) f = \Omega(f), \qquad (1)$$

where f is the density probability distribution of finding a particle with velocity $\boldsymbol{\xi}$ at position $\boldsymbol{x}$ at time t. The macroscopic observables are as usual given in terms of moments of f

$$\rho = \int \mathrm{d}\boldsymbol{\xi}\ f, \quad \rho\boldsymbol{u} = \int \mathrm{d}\boldsymbol{\xi}\ \boldsymbol{\xi} f. \qquad (2)$$

With $\mathcal{G}$ a convolution filter kernel, and denoting the filtered counterpart of any quantity, a, as $\overline{a} \equiv \mathcal{G} * a$, one can write the filtered Boltzmann equation as

$$\frac{\mathrm{d}\overline{f}}{\mathrm{d}t} = \overline{\Omega(f)} \Leftrightarrow \frac{\mathrm{d}\overline{f}}{\mathrm{d}t} - \Omega(\overline{f}) = \mathcal{R}, \qquad (3)$$

where $\mathcal{R} \equiv \overline{\Omega(f)} - \Omega(\overline{f})$ corresponds to the subgrid term that has to be modeled and represents the error of the commutator of the collision and the filtering operators.

B. Approximate deconvolution method and lattice Boltzmann method

We now use the idea developed by Stolz and Adams[18–20] of trying to reconstruct the unfiltered-filtered fields in an approximate manner. To this aim we define an easy to compute inverse filter approximation $\mathcal{Q}$

$$\mathcal{Q} * \mathcal{G} = I + \mathcal{O}(h^l), \qquad (4)$$

where I is the identity, h a measure of the grid resolution and $l > 0$ the order of the reconstruction. Defining $f^* \equiv \mathcal{Q} * \overline{f}$, one can rewrite the r.h.s. of Eq. (3) following the approach by Mathew *et al.*[23],

$$\mathcal{R} = \mathcal{R}_1 + \mathcal{R}_2 = \overline{\Omega\left(f^*\right)} - \Omega\left(\overline{f}\right) + \overline{\Omega(f)} - \overline{\Omega\left(f^*\right)}, \text{ where} \qquad (5)$$

$$\mathcal{R}_1 \equiv \overline{\Omega\left(f^*\right)} - \Omega\left(\overline{f}\right), \quad \mathcal{R}_2 \equiv \mathcal{G} * \left[\Omega(f) - \Omega\left(f^*\right)\right]. \qquad (6)$$

We will now focus our attention on $\mathcal{R}_2$, the part of $\mathcal{R}$ that needs to be modeled. Under the assumption that $|f - f^*| \ll 1$, one can do a Taylor expansion of $\Omega(f^*)$ around f up to order one

$$\mathcal{R}_2 \cong -\mathcal{G}*\left[\partial_{f^*}\Omega\big|_f (f^* - f)\right] = \mathcal{G}*\left[\partial_{f^*}\Omega\big|_f (\mathcal{Q}*\mathcal{G} - I) * f\right]. \qquad (7)$$

Inspired by the work of Mathew *et al.*[23] one replaces f by f^* to close this equation

$$\mathcal{R}_2 \cong -\mathcal{G} * \left[(\mathcal{Q}*\mathcal{G} - I) * f^* \partial_{f^*}\Omega\big|_{f=f^*}\right]. \qquad (8)$$

The assumption $|f - f^*| \ll 1$ is actually true only if the filter width is in the dissipation range which is true only if the simulation is completely resolved. In our case we rather have that the large scales of f are close to those of f^* and since we are aiming for a model for the resolved scales the Taylor expansion remains valid.

With this approximation one can rewrite Eq. (3) as

$$\mathcal{G}*\left(\frac{\mathrm{d}f^*}{\mathrm{d}t} - \Omega\left(f^*\right)\right) = \mathcal{G}*\left[\left(I - \mathcal{Q}*\mathcal{G}\right)*f^*\partial_{f^*}\Omega\Big|_{f=f^*}\right]. \tag{9}$$

Specifying now the collision operator as the standard BGK (Bhatnagar, Gross and Krook[24]), and following the standard velocity discretization procedure of the Boltzmann-BGK equation proposed in Shan *et al.*[25] (see also Ref. 26) Eq. (9) reads

$$\mathcal{G}*\left(\frac{\mathrm{d}f^*}{\mathrm{d}t} + \omega\left(f_i^* - f_i^{(0)}(f^*)\right)\right) = \underbrace{-\omega\mathcal{G}*\left[\sum_j \partial_{f_j^*}\left(f_i^* - f_i^{(0)}(f^*)\right)\Big|_{f=f^*}\left(I - \mathcal{Q}*\mathcal{G}\right)*f_j^*\right]}_{\equiv\mathcal{R}_{i,\mathrm{bgk}}}, \tag{10}$$

where ω is the relaxation frequency, $f_i^* \equiv f^*(\boldsymbol{x}, \boldsymbol{\xi}_i, t)$ is the velocity-discretized distribution function (with $\boldsymbol{\xi}_i$ the q abscissae of the Gauss–Hermite quadrature), the $f_i^{(0)}(f^*)$ are the Hermite expanded Maxwell distribution up to an arbitrary order (corresponding to the Gauss–Hermite quadrature order) evaluated with the moments of $\{f_k^*\}_{k=0}^{q-1}$.

When truncating the Hermite expansion of the equilibrium distribution up to order two, the macroscopic limit of the BGK equation gives asymptotically the weakly compressible Navier–Stokes equations (see Ref. 27). The equilibrium distribution is then found to be

$$f_i^{(0)}(f) = w_i\rho\left(1 + \frac{\boldsymbol{\xi}_i\cdot\boldsymbol{u}}{c_s^2} + \frac{1}{2c_s^4}\mathcal{H}_i^{(2)} : \boldsymbol{u}\boldsymbol{u}\right), \tag{11}$$

where $\rho = \sum_i f_i$, $\boldsymbol{j} \equiv \rho\boldsymbol{u} = \sum_i \boldsymbol{\xi}_i f_i$, ":" is the full index contraction and $\mathcal{H}_i^{(2)} \equiv \boldsymbol{\xi}_i\boldsymbol{\xi}_i - c_s^2\boldsymbol{I}$ ($\boldsymbol{I}$ being the identity, w_i and c_s the weights and the speed of sound of the lattice). Defining $\Delta a \equiv (I - \mathcal{Q}*\mathcal{G})*a$ (a being an arbitrary quantity), and specifying

$f_i^{(0)}$ allows us to evaluate $\mathcal{R}_{i,\mathrm{bgk}}$ (see Eq. (10))

$$\mathcal{R}_{i,\mathrm{bgk}} = \sum_j \partial_{f_j^*} \Bigg[f_i^* - w_i \Bigg(\sum_k f_k^* + \frac{\boldsymbol{\xi}_i}{c_s^2} \cdot \sum_k \boldsymbol{\xi}_k f_k^* + \frac{1}{2c_s^4} \left(\sum_m f_m^* \right)^{-1} \mathcal{H}_i^{(2)} : \sum_k \boldsymbol{\xi}_k f_k^* \sum_l \boldsymbol{\xi}_l f_l^* \Bigg) \Bigg]_{f=f^*} \Delta f_j^* \tag{12}$$

$$= \sum_j \Bigg[\delta_{ij} - w_i \Bigg(\sum_k \delta_{jk} + \frac{\boldsymbol{\xi}_i \cdot \boldsymbol{\xi}_j}{c_s^2} + \frac{1}{2c_s^4} \mathcal{H}_i^{(2)} : \Bigg(- \left(\sum_m f_m \right)^{-2} \sum_n \delta_{nj} \sum_k \boldsymbol{\xi}_k f_k \sum_l \boldsymbol{\xi}_l f_l + \left(\sum_m f_m \right)^{-1} \boldsymbol{\xi}_j \sum_l \boldsymbol{\xi}_l f_l + \left(\sum_m f_m \right)^{-1} \sum_l \boldsymbol{\xi}_l f_l \boldsymbol{\xi}_j \Bigg) \Bigg) \Bigg]_{f=f^*} \Delta f_j^* \tag{13}$$

$$= \Delta f_i^* - w_i \Bigg(\Delta\rho^* + \frac{\boldsymbol{\xi}_i \cdot (\Delta \boldsymbol{\jmath}^*)}{c_s^2} + \frac{1}{2c_s^4} \mathcal{H}_i^{(2)} : \left(- \frac{\Delta\rho^*}{\rho^{*2}} \boldsymbol{\jmath}^* \boldsymbol{\jmath}^* + \frac{1}{\rho^*} \Delta\boldsymbol{\jmath}^* \boldsymbol{\jmath}^* + \frac{1}{\rho^*} \boldsymbol{\jmath}^* \Delta\boldsymbol{\jmath}^* \right) \Bigg) \tag{14}$$

Therefore Eq. (10) becomes

$$\mathcal{G} * \left(\frac{\mathrm{d}f^*}{\mathrm{d}t} + \omega \left(f_i^* - f_i^{(0)}(f^*) \right) \right) = -\omega \mathcal{G} * \mathcal{R}_{i,\mathrm{bgk}}. \tag{15}$$

This last equation is the complete ADM-BGK equation. Following the conclusions of Mathew *et al.*[23], the $\mathcal{R}_2$ term can be neglected without noticeable effects on the results of the simulations to obtain a further simplified model

$$\mathcal{G} * \left(\frac{\mathrm{d}f^*}{\mathrm{d}t} - \Omega\left(f^*\right) \right) = 0. \tag{16}$$

The advantage of this approximation is that the implementation is completely straightforward since, apart from the filtering step, the LBM time marching scheme remains *exactly* the same as for DNS computations. We therefore have the normal collide-and-stream process followed by the filtering operation (the implementation details are discussed later).

C. Chapman–Enskog expansion of the ADM-BGK equation

In this section the Chapman–Enskog (CE) expansion of the ADM-BGK equation is discussed. The CE expansion is based on the assumption that the non-filtered distribution function is given by its local equilibrium value to which a small perturbation (proportional to the Knudsen number) is added

$$f_i = f_i^{(0)} + f_i^{(1)}, \quad f_i^{(1)} \ll f^{(0)}. \tag{17}$$

Here our formulation of the BGK equation is based on the approximate deconvolution of the distribution function. We therefore want to write their CE equivalent for f_i^*

$$f_i^* = \mathcal{Q} * \mathcal{G} * f_i = \left(f_i^{(0)} \right)^* + \left(f_i^{(1)} \right)^*. \tag{18}$$

The difference between the approximate deconvolution and the "bare" distribution functions is of order $\mathcal{O}(h^l)$ (see Eq. (4)). Since, the LBM is known to be second order accurate in space, $\mathcal{O}(h^2)$ (see Refs. 26–28), by choosing carefully the filter and the deconvolution one can argue that the difference between $f_i^{(0)}(f^*)$ and $(f_i^{(0)})^*$ (and thus between

$f_i^{(1)}(f^*)$ and $(f_i^{(1)})^*)$ can be made smaller than the order of the method

$$f_i^* \cong f_i^{(0)}(f^*) + f_i^{(1)}(f^*). \tag{19}$$

Therefore the CE expansion of the ADM–BGK equation is very similar to what can be found is the literature (see Refs. 27 and 29 for more details).

Taking the zeroth and first order moment of Eq. (15), one gets

$$\partial_t \rho^* + \boldsymbol{\nabla}\cdot\boldsymbol{j}^* = -\omega\sum_i \mathcal{R}_{i,\mathrm{bgk}}, \tag{20}$$

$$\partial_t \boldsymbol{j}^* + \boldsymbol{\nabla}\cdot\left(\frac{\boldsymbol{j}^*\boldsymbol{j}^*}{\rho^*}\right) + \boldsymbol{\nabla}\cdot\boldsymbol{P}^* = -\omega\sum_i \boldsymbol{\xi}_i\mathcal{R}_{i,\mathrm{bgk}}, \tag{21}$$

where $\boldsymbol{P}^* = \sum_i(\boldsymbol{\xi}_i - \boldsymbol{j}^*/\rho^*)(\boldsymbol{\xi}_i - \boldsymbol{j}^*/\rho^*)f_i^*$. Replacing f_i^* by their CE expansion and keeping only the lower order terms in Eq. (15), one gets (for simplicity we apply $\mathcal{G}^{-1}$ on both sides of the equation and the dependence on f^* is understood in $f_i^{(0)}$ and $f_i^{(1)}$)

$$\begin{aligned}\frac{\mathrm{d}f_i^{(0)}}{\mathrm{d}t} + \omega f_i^{(1)} &= -\omega\left[\Delta f_i^{(0)} - w_i\left(\Delta\rho^* + \frac{\boldsymbol{\xi}_i\cdot(\Delta\boldsymbol{j}^*)}{c_s^2}\right.\right.\\ &\qquad \left.\left. + \frac{1}{2c_s^4}\mathcal{H}_i^{(2)} : \left(-\frac{\Delta\rho^*}{\rho^{*2}}\boldsymbol{j}^*\boldsymbol{j}^* + \frac{1}{\rho^*}\Delta\boldsymbol{j}^*\boldsymbol{j}^* + \frac{1}{\rho^*}\boldsymbol{j}^*\Delta\boldsymbol{j}^*\right)\right)\right]\\ &= -\frac{w_i\omega}{2c_s^4}\mathcal{H}_i^{(2)} : \left[\Delta\left(\frac{\boldsymbol{j}^*\boldsymbol{j}^*}{\rho^*}\right) + \frac{\Delta\rho^*}{\rho^{*2}}\boldsymbol{j}^*\boldsymbol{j}^* - \frac{1}{\rho^*}\Delta\boldsymbol{j}^*\boldsymbol{j}^* - \frac{1}{\rho^*}\boldsymbol{j}^*\Delta\boldsymbol{j}^*\right].\end{aligned} \tag{22}$$

where in the second line we used that

$$f_i^{(0)}(f^*) = w_i\left(\rho^* + \frac{\boldsymbol{\xi}_i\cdot\boldsymbol{j}^*}{c_s^2} + \frac{1}{2c_s^4}\mathcal{H}_i^{(2)} : \frac{\boldsymbol{j}^*\boldsymbol{j}^*}{\rho^*}\right). \tag{23}$$

Taking the zeroth and first order moments of Eq. (22) one finds the equivalent of Euler equations

$$\partial_t\rho^* + \boldsymbol{\nabla}\cdot\boldsymbol{j}^* = 0, \tag{24}$$

$$\partial_t\boldsymbol{j}^* + \boldsymbol{\nabla}\cdot\left(\frac{\boldsymbol{j}^*\boldsymbol{j}^*}{\rho^*}\right) = -\boldsymbol{\nabla}p^*, \tag{25}$$

where $p^* = c_s^2\rho^*$. To go to the Navier–Stokes level, the evaluation of the second order moment of Eq. (22) is needed. After some tedious algebra one finds

$$\begin{aligned}\sum_i \mathcal{H}_i^{(2)} f_i^{(1)} = -\frac{c_s^2}{\omega}\rho^*&\left[\boldsymbol{\nabla}\left(\frac{\boldsymbol{j}^*}{\rho^*}\right) + \left(\boldsymbol{\nabla}\left(\frac{\boldsymbol{j}^*}{\rho^*}\right)\right)^{\mathrm{T}}\right]\\ &+ \Delta\left(\frac{\boldsymbol{j}^*\boldsymbol{j}^*}{\rho^*}\right) + \frac{\Delta\rho^*}{\rho^{*2}}\boldsymbol{j}^*\boldsymbol{j}^* - \frac{1}{\rho^*}\Delta\boldsymbol{j}^*\boldsymbol{j}^* - \frac{1}{\rho^*}\boldsymbol{j}^*\Delta\boldsymbol{j}^*\end{aligned} \tag{26}$$

where the superscript "T" stands for the transpose operation. Finally, setting $\boldsymbol{P}^* = \sum_i(\boldsymbol{\xi}_i - \boldsymbol{j}^*/\rho^*)(\boldsymbol{\xi}_i - \boldsymbol{j}^*/\rho^*)(f_i^{(0)} + f_i^{(1)})$ in Eq. (21), the Navier–Stokes limit of the ADM-BGK equation reads

$$\begin{aligned}\partial_t\boldsymbol{j}^* + \boldsymbol{\nabla}\cdot\left(\frac{\boldsymbol{j}^*\boldsymbol{j}^*}{\rho^*}\right) =& -\boldsymbol{\nabla}p^* + 2\mu\boldsymbol{\nabla}\cdot\boldsymbol{S}^*\\ &- \boldsymbol{\nabla}\cdot\left(\Delta\left(\frac{\boldsymbol{j}^*\boldsymbol{j}^*}{\rho^*}\right) + \frac{\Delta\rho^*}{\rho^{*2}}\boldsymbol{j}^*\boldsymbol{j}^* - \frac{1}{\rho^*}\Delta\right.\end{aligned} \tag{27}$$

where $\mu = -c_s^2\rho^*/\omega$ and $\boldsymbol{S}^* = (\boldsymbol{\nabla}(\boldsymbol{j}^*/\rho^*) + \boldsymbol{\nabla}(\boldsymbol{j}^*/\rho^*)^{\mathrm{T}})/2$. This equation corresponds to Eq. (A2) of the work by Mathew *et al.*[23].

When using the simplified collision of Eq. (16) the momentum conservation equation is reduced to

$$\partial_t\boldsymbol{j}^* + \boldsymbol{\nabla}\cdot\left(\frac{\boldsymbol{j}^*\boldsymbol{j}^*}{\rho^*}\right) = -\boldsymbol{\nabla}p^* + 2\mu\boldsymbol{\nabla}\cdot\boldsymbol{S}^*. \tag{28}$$

In what follows we will only consider the simplified model.

D. Implementation of the ADM-BGK equation

After discretization of time and space using the standard trapezoidal rule and change of variables (see Ref. 30), the algorithm for the simulation of weakly compressible fluids, is therefore given by

1. Standard collide and stream process ($\delta x = \delta t = 1$)

$$f_i^{*\mathrm{out}}(\boldsymbol{x}+\boldsymbol{\xi}_i, t+1) = f_i^{*\mathrm{in}}(\boldsymbol{x}, t) - \omega \left(f_i^{*\mathrm{in}}(\boldsymbol{x}, t) - f_i^{(0)^*}(\boldsymbol{x}, t) \right), \tag{29}$$

where ω is the relaxation frequency

$$f_i^{(0)^*} = w_i \left(\rho^* + \frac{\boldsymbol{\xi}_i \cdot \boldsymbol{j}^*}{c_s^2} + \frac{\mathcal{H}_i^{(2)}}{2c_s^4} : \frac{\boldsymbol{j}^* \boldsymbol{j}^*}{\rho^*} \right), \tag{30}$$

and where $\rho^* = \sum_i f_i^{*\mathrm{in}}$, $\boldsymbol{j}^* = \sum_i \boldsymbol{\xi}_i f_i^{*\mathrm{in}}$.

2. Application of the explicit filtering operation

$$f_i^{*\mathrm{in}} = \mathcal{Q} * \mathcal{G} * f_i^{*\mathrm{out}}, \quad \forall i. \tag{31}$$

The ADM operator $\mathcal{Q} * \mathcal{G}$ is described in more details in the next subsection.

In the collision–streaming steps we used the order two truncation of the equilibrium distribution function in Hermite polynomials in order to simulate weakly compressible fluids. The reader should be aware that the ADM is independent of this choice and therefore can be extended straightforwardly to compressible and thermal flows by changing the truncation order of the equilibrium as well as the lattice definition (see Ref. 25).

E. Description of the filters used

The filtering operation is done with the filters proposed in Ricot *et al.*[31]. They are given by

$$\mathcal{Q} * \mathcal{G} * f_i^* = f_i^*(\boldsymbol{x}, t) - \sigma \sum_{j=1}^{D} \sum_{n=-N}^{N} d_n f_i^* \left(\boldsymbol{x} + n\boldsymbol{e}_j, t \right), \tag{32}$$

where the $\boldsymbol{e}_i$ are the D-dimensional Cartesian basis vectors, $2N+1$ is the number of points of the filter stencil, and $\sigma \in [0, 1]$ is the filter strength. The $d_n = d_{-n}$ are obtained by canceling the Taylor expansion of the last term of r.h.s. of this last equation and canceling order by order up to the desired expansion order N

$$\sum_{n=-N}^{N} n^k d_n = 0, \quad 0 \leq k \leq 2N+1. \tag{33}$$

The values for the d_n coefficients are given in Table I for different N values. The ADM operation is therefore non-local since it needs to access N neighbors in each D direction for all the q discrete velocities $\boldsymbol{\xi}_i$.

Finally, for the sake of clarity, let us write down the 3-points filter ADM operator in $1D$

N	d_0	d_1	d_2	d_3	d_4
1	1/2	-1/4			
2	6/16	-4/16	1/16		
3	5/16	-15/64	3/32	-1/64	
4	35/128	-7/32	7/64	-1/32	1/256

TABLE I. The filter weights for stencils up to 9 points ($N = 4$).

(the procedure is straightforwardly applicable for larger filters and higher dimensions)

$$\begin{aligned} f_i^{*\mathrm{in}}(x,t) &= f_i^{*\mathrm{out}}(x,t) - \sigma \sum_{n=-1}^{1} d_n f_i^{*\mathrm{out}}(x+n,t) \\ &= f_i^{*\mathrm{out}}(x,t) - \sigma \left(d_{-1} f_i^*(x-1,t) + d_0 f_i^*(x,t) + d_1 f_i^*(x+1,t)\right) \end{aligned} \tag{34}$$

As can be seen form this expression for the ADM operator, the implementation remains easy although adding a non-negligible amount of computations.

The choice of the filters used here is not unique. In general any invertible filter $\mathcal{G}$ that satisfies the condition

$$\mathcal{G} * a = \int_{-\infty}^{\infty} \mathrm{d}\boldsymbol{y}\ \mathcal{G}(\boldsymbol{x}-\boldsymbol{y}) a(\boldsymbol{y}) \tag{35}$$

could be used. In our case since we are directly computing with $Q * \mathcal{G}$, we only need to know the difference between the filter and its inverse with respect to the unity. Therefore the invertibility condition might be a bit weaker.

III. THE TIME DEPENDENT MIXING LAYER

In this section we propose to study the applicability of the LBM-ADM technique for LES simulations on a well know benchmark where there exists a sufficiently large amount of data. We will study different filters and σ values.

A. Numerical setup

The simulation is initialized with a velocity field of (see Fig. 1)

$$u_x = \frac{1}{2}\delta U \left(1 + \mathrm{erf}\left(\frac{y}{\sqrt{2\pi}\delta_0}\right)\right), \quad u_y = 0, \quad u_z = 0. \tag{36}$$

where δU is the difference of velocity between the two layers, δ_0 the initial momentum thickness, and erf the error function

$$\mathrm{erf}(x) = \frac{2}{\sqrt{\pi}} \int_0^x \mathrm{d}t e^{-t^2}. \tag{37}$$

The momentum thickness δ_m is defined as

$$\delta_m = \int_{-\infty}^{\infty} \mathrm{d}y \left(\frac{1}{4} - \frac{u_x^2}{\delta U^2}\right) \tag{38}$$

and the initial Reynolds number based on the momentum thickness is $\mathrm{Re} = \delta U \delta_0 / \nu = 800$. The flow is periodic in the spanwise and streamwise directions, while a free-slip boundary condition is imposed on the y-boundaries. This flow exhibits a turbulent behavior after the appearance of a Kelvin–Helmholtz instability (see Ref. 32). When the

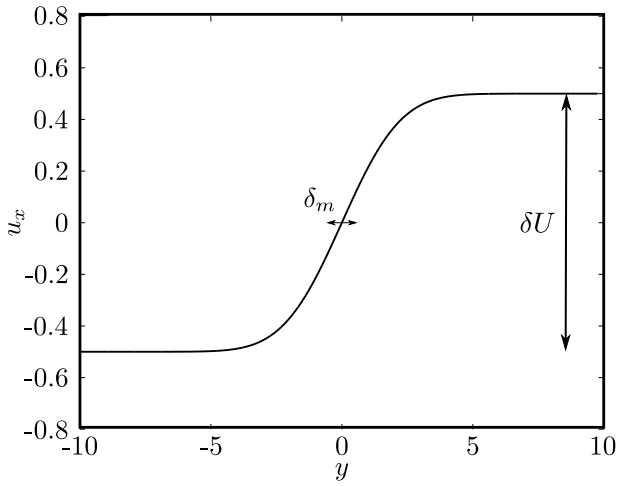

FIG. 1. The horizontal velocity profile with respect to y, for $\delta U = 1$ and $\delta_m = 1$.

turbulence is correctly established, one obtains a self-similar behavior of the flow and a constant growth of the momentum thickness δ_m with respect to the non-dimensional time, $\tau \equiv t\delta U/\delta_m$, is expected. The Kolmogorov inertial range is observed after the second pairing of the quasi-2D Kelvin-Helmholtz rolls, when the initial condition yields the growth of these structures. In order to trigger the Kelvin–Helmholtz instability a perturbation is superimposed on the initial velocity profile (see Ref. 33 for a detailed description of the perturbation). It consists of a dephased series of sines and cosines that will excite the first more unstable modes. This perturbation is modulated by a Gaussian centered on $y = 0$ with standard deviation δ_0. The amplitude of the perturbation is equal to $0.1\delta U$.

The regular grid resolutions used for the simulations presented hereafter are given by $(64M)^3$, with $M = 1, 2, 4$ where M corresponds to the initial momentum thickness. The velocity difference in lattice units was chosen to be $\delta U = 0.05$. Simulations have been performed with filters with $N = 2, 3, 4$. Furthermore we chose to use different filter strengths $\sigma = 0.005, 0.05, 0.5$. For these grid sizes the DNS performed with the standard LBGK model are becoming numerically unstable when the transition towards turbulence occurs. A comparison is made for the same resolutions with an LBM model using the Smagorinsky model (see Ref. 9) for the details of implementation of the model, where the eddy viscosity, ν_t, is given by

$$\nu_t = (C\overline{\Delta})^2 ||\boldsymbol{S}||, \tag{39}$$

where C is the Smagorinsky constant, $\overline{\Delta}$ is the filter width, and $\boldsymbol{S} = (\boldsymbol{\nabla u} + (\boldsymbol{\nabla u})^{\mathrm{T}})/2$ is the strain rate tensor and $||\boldsymbol{S}|| \equiv \sqrt{2S_{\alpha\beta}S_{\alpha\beta}}$, where Einstein's summation convention is understood. In this work $C = 0.14$ was chosen.

B. Results

The following results are obtained using the parallel open source library Palabos (see http://www.palabos.org). The lattice used is the standard D3Q19 (see Ref. 25 for a complete description). On Fig. 2 one can see

snapshots of the simulation at times, $t = 0, 125, 250, 375, 500$. There, the x-component of the velocity and the iso-surfaces of the Q-criterion (different at each time) are depicted. The initial perturbation at time $t = 0$ slowly develops into a turbulent flow after $t \cong 250$, and one can see the well known worm-like structures forming. The filters width as well as their strength must be carefully chosen, in order to allow the instability to develop properly. To our knowledge there exist no way to determine them a priori but must be tuned depending on the physical problem under consideration. For instance, in our case, the $N = 1$ (three points) filter never exhibits a turbulent behavior. While in the case of the $N = 2$ the development of turbulence can be observed but not for any value of σ. The $\sigma = 0.5, 0.05, 0.005$ strengths are depicted in Fig. 3, where one can see that for $\sigma = 0.5, 0.05$ the increase rate of the momentum thickness seems way too underestimated, indicating that the Kelvin–Helmholtz instability is never initiated and the subsequent turbulent behavior never occurs. On the contrary, for $\sigma = 0.005$, the self-similar period is present.

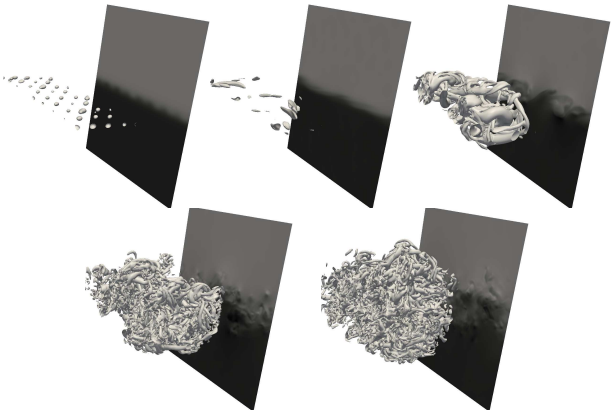

FIG. 2. Iso-surfaces of the Q-criterion and u_x at times $t = 0, 125, 250, 375, 500$ (from left to right and top to bottom). In black the velocity is negative while it is positive in light gray.

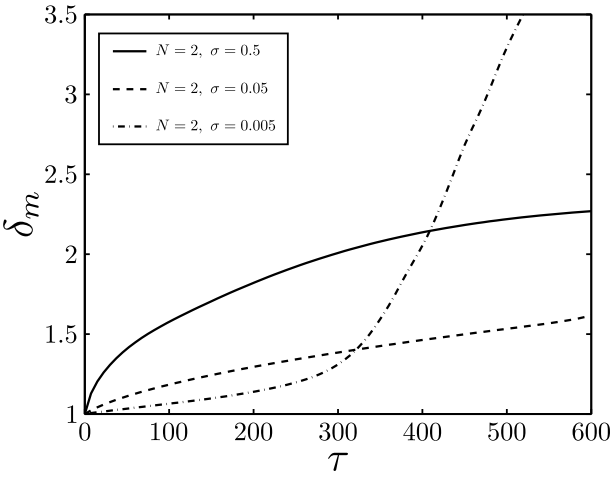

FIG. 3. The momentum thickness with respect to the normalized time $\tau = t\delta U/\delta_m$ for $N = 2$ and $\sigma = 0.5, 0.05, 0.005$.

In order to validate that the simulation is converging with the grid resolution, we performed a series of measurements for $M = 1, 2, 4$ (resolutions of $64^3, 128^3, 256^3$) for all filter widths for $\sigma = 0.005$. As can be seen from Fig. 4 the increase rate of the momentum thickness is very similar for all simulations. The main difference is the moment where the instability is initiated. From now

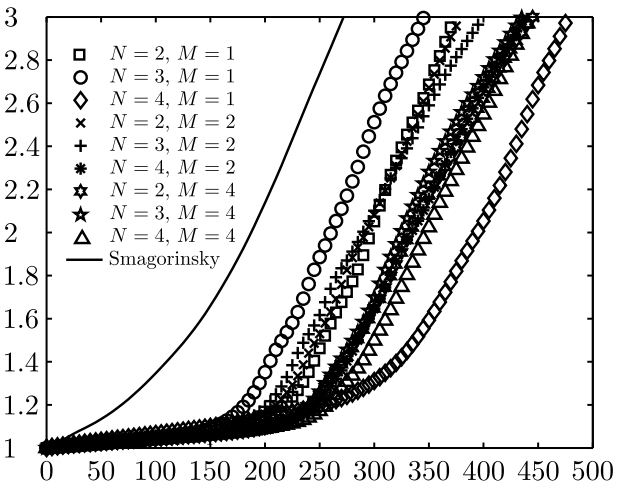

FIG. 4. The momentum thickness with respect with the non-dimensional time $\tau = t\delta U/\delta_m$ for $N = 2, 3, 4$ and $\sigma = 0.005$ for $M = 1, 2, 4$ as well as for the Smagorinsky model for $M = 1$.

on, only the case of $M = 1$ is considered.

In the work by Rogers and Moser[32], the growth rate $r = \mathrm{d}\delta_m/\mathrm{d}\tau$ was found to be $r = 0.014$ in agreement with the experimental data of Dimotakis[34] (0.014-0.021). In the present study, the value of r varies slightly depending on the filters width as shown in Table II. While the analytical models proposed here are completely generic a specific filter has been chosen for implementation purposes.

The self similar behavior is also confirmed by the fact that instantaneous averaged velocity profiles $\langle u_x(\overline{y})\rangle$ and the r.m.s. velocity $\langle u_x'(\overline{y})^2\rangle$, where $\overline{y} \equiv y/\delta_m(t)$, are superimposed for five times (see Figs 5 and 6).

On Fig. 7 the one dimensional energy spectrum with respect to the k_x is depicted. It can be seen that the expected $k_x^{-5/3}$ energy slope is relatively well recovered. The spectrum of the 5 and 7-points filter seems to be a bit "off" the $-5/3$ slope while the 9-points filter gives better result, which seem even a bit closer to the $k_x^{-5/3}$ than those obtained using the the Smagorinsky model.

	$N = 2$	$N = 3$	$N = 4$	Smagorinsky
r	0.012	0.013	0.013	0.013

TABLE II. Value of the momentum thickness growth rate r for the different filters width and for the Smagorinsky model.

IV. CONCLUSION

In the present paper we applied the approximate deconvolution model to the lattice Boltzmann method. We proposed two levels of approximation for the closure of the deconvoluted equation. We showed that the simplified ADM-LBM model represents correctly the dynamics of turbulent flows by simulating the turbulent mixing layer. The self-similar behavior as well as the energy spectrum is recovered correctly with a limited amount of grid points.

The ADM–LBM has the advantage of not relying on "extrapolations" of Navier–Stokes turbulence models applied to the LBM, since

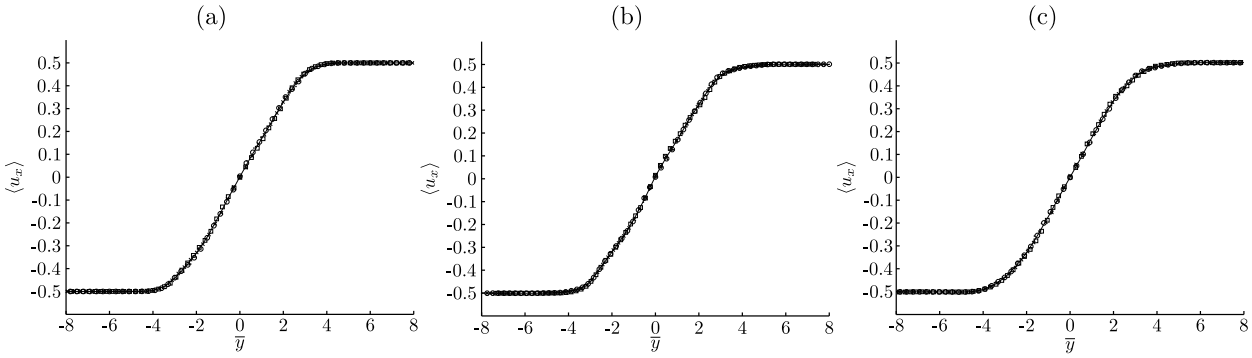

FIG. 5. The average velocity x-component $\langle u_x \rangle$ with respect to the rescaled y-coordinate $\overline{y}$ for filter widths (a) $N = 2$ (b) $N = 3$ and (c) $N = 4$ for five times between in the self-similar region.

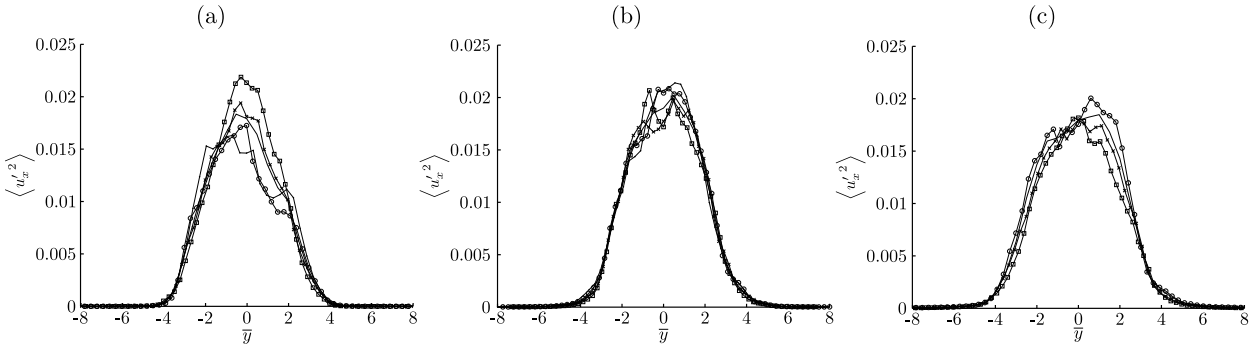

FIG. 6. The average rms velocity x-component $\langle u_x'^2 \rangle$ with respect to the rescaled y-coordinate $\overline{y}$ for filter widths (a) $N = 2$ (b) $N = 3$ and (c) $N = 4$ for five times in the self-similar period.

the approximate deconvolution method is applied directly on the distribution functions. It is therefore possible to model the dynamics of turbulence on a mesoscopic level and offers an alternate methodology compared to standard LBM-LES techniques. The proposed algorithm keeps the simplicity of the LBM by adding a simple ADM step, allowing this approach to be applied in a straightforward fashion to any kind LBM models for advection–diffusion or thermal compressible flows among others. It is worth keeping in mind that, varying the truncation order of the Hermite expansion of the collision term, an infinite hierarchy of physical flow models is recovered: Euler equations, weakly compressible athermal Navier-Stokes equations, compressible thermal Navier-Stokes equations, Burnett equations, super-Burnett equations ... Therefore, the proposed methodology allows for a practical derivation of closed LES-type equations for these embedded models.

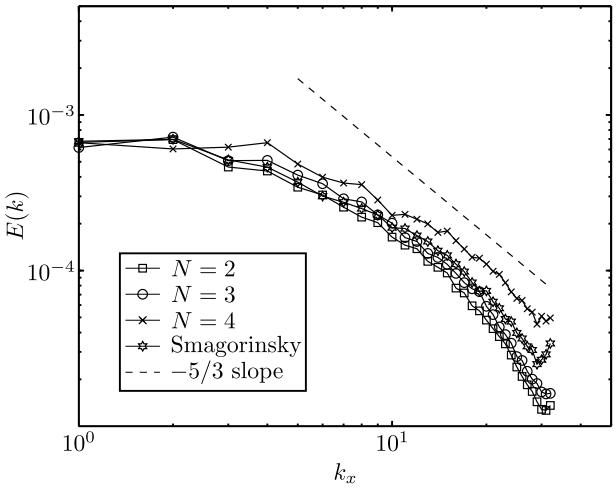

FIG. 7. The instantaneous energy spectrum $E(k)$ with respect to k_x and the expected $k_x^{-5/3}$ slope.

Extending LES to higher-order models, such as Burnett equations, the relative influence of the $\mathcal{R}_2$ term and the required filter strength need to be re-investigated.

In principle, the method could also be extended to multiple relaxation time models and not only be restricted to the standard BGK. In the same way, the proposed Approximate Deconvolution approach makes it easy to handle non-linear source terms.

An actual implementation of Eq. (15) and a comparison with the simplified model implemented in the present work is left for future work. Furthermore, as suggested in previous papers dealing with the Navier–Stokes framework the filters used seem to have an influence on the resolved scales, especially in wall-bounded flows in which turbulence-generating instabilities are dissipation-dependent. Such effects might be interesting to test on the LBM–ADM.

ACKNOWLEDGEMENTS

O. Malaspinas would like to thankfully acknowledge the support of the Swiss National Science Foundation SNF (Award PBELP2-133356) and the Department of Theoretical Physics of the University of Geneva for allowing the use of the *Andromeda* cluster. Pierre Sagaut acknowledges the support of FUI via the LaBS project.

REFERENCES

[1]P. Sagaut, *Large Eddy Simulation for Incompressible Flows: An Introduction* (Springer, Berlin, 2001).

[2]E. Garnier, N.A. Adams, and P. Sagaut, *Large Eddy Simulation for Compressible Flows* (Springer, Berlin, 2009).

[3]P. Sagaut, S. Deck, and M. Terracol, *Multiscale and Multiresolution Approaches in turbulence* (Imperial College Press, London, 2009).

[4]J. Smagorinsky, "General circulation experiments with the primitive equations: I. the basic equations," Mon. Weather Rev. **91**, 99–164 (1963).

[5]O. Labbé,E. Montreuil,P. Sagaut, "Large-eddy simulation of heat transfer over a backward facing step," Int. J. Numer. Heat Transfer - Part A. **42**, 73–90 (2002).

[6]C. Seror,P. Sagaut,C. Bailly,D. Juvé, "On the radiated noise computed by Large-eddy simulation," Phys. Fluids **13**, 476–487 (2001).

[7]P. Quéméré,P. Sagaut,V. Couaillier, "A new multidomain/multiresolution method for large-eddy simulation," Int. J. Numer. Methods Fluids **36**, 391–416 (2001).

[8]P. Quéméré,P. Sagaut, "Zonal multidomain RANS/LES simulation of turbulent flows," Int. J. Numer. Methods Fluids **40**, 903–925 (2002).

[9]S. Hou, J. Sterling, S. Chen, and G. D. Doolen, "A lattice Boltzmann subgrid model for high Reynolds number flows," Fields Inst. Comm. **6**, 151–66 (1996).

[10]Jack G. M. Eggels, "Direct and large-eddy simulation of turbulent fluid flow using the lattice-Boltzmann scheme," Int. J. Heat Fluid Flow **17**, 307 – 323 (1996).

[11]O. Filippova, S. Succi, F. Mazzocco, C. Arrighetti, G. Bella, and D. Hänel, "Multiscale lattice Boltzmann schemes with turbulence modeling," J. Comp. Phys. **170**, 812 – 829 (2001).

[12]M. Krafczyk, J. Tölke, and L.-S. Luo, "Large-eddy simulations with a multiple-relaxation-time LBE model," Int. J. Mod. Phys. B **17**, 33–39 (2003).

[13]J. Kerimo and S. Girimaji, "Boltzmann-BGK approach to simulating weakly compressible 3D turbulence: comparison between lattice Boltzmann and gas kinetic methods," J. Turbul. **8** (2007).

[14]Y.-H. Dong, P. Sagaut, and S. Marié, "Inertial consistent subgrid model for large-eddy simulation based on the lattice Boltzmann method," Phys. Fluids **20**, 035104 (2008)

[15]K. N. Premnath, M. J. Pattison, and S. Banerjee, "Dynamic subgrid scale modeling of turbulent flows using lattice-Boltzmann method," Physica A **388**, 2640 – 2658 (2009).

[16]S. Chen, "A large-eddy-based lattice Boltzmann model for turbulent flow simulation," Appl. Math. Comput. **215**, 591 – 598 (2009).

[17]M. Weickert, G. Teike, O. Schmidt, and M. Sommerfeld, "Investigation of the LES WALE turbulence model within the lattice Boltzmann framework," Comput. Math. Appl. **59**, 2200 – 2214 (2010).

[18]S. Stolz and N. A. Adams, "An approximate deconvolution procedure for large-eddy simulation," Phys. Fluids **11**, 1699–1701 (1999).

[19]S. Stolz, N. A. Adams, and L. Kleiser, "An approximate deconvolution model for large-

eddy simulation with application to incompressible wall-bounded flows," Phys. Fluids **13**, 997–1015 (2001).

[20]S. Stolz, N. A. Adams, and L. Kleiser, "The approximate deconvolution model for large-eddy simulations of compressible flows and its application to shock-turbulent-boundary-layer interaction," Phys. Fluids **13**, 2985–3001 (2001).

[21]M.S. Loginov, N.A. Adams, and A.A. Zheldotov, "Large-eddy simulation of shock wave/turbulent boundary layer interaction," J. Fluid Mech. **565**, 135–169 (2009).

[22]P. Sagaut, "Toward advanced subgrid models for Lattice-Boltzmann-based large-eddy simulation: Theoretical formulations," Comput. Math. Appl. **59**, 2194 – 2199 (2010).

[23]J. Mathew, R. Lechner, H. Foysi, J. Sesterhenn, and R. Friedrich, "An explicit filtering method for large eddy simulation of compressible flows," Phys. Fluids **15**, 2279–2289 (2003).

[24]P. L. Bhatnagar, E. P. Gross, and M. Krook, "A model for collision processes in gases. i. small amplitude processes in charged and neutral one-component systems," Phys. Rev. **94**, 511–525 (May 1954).

[25]X. Shan, X.-F. Yuan, and H. Chen, "Kinetic theory representation of hydrodynamics: a way beyond the Navier-Stokes equation," J. Fluid Mech. **550**, 413–441 (2006).

[26]O. Malaspinas, *Lattice Boltzmann method for the simulation of viscoelastic fluid flows*, PhD dissertation, EPFL, Lausanne, Switzerland (2009), http://library.epfl.ch/theses/?nr=4505.

[27]S. Chen and G. D. Doolen, "Lattice Boltzmann method for fluid flows," Ann. Rev. Fluid Mech. **30**, 329–364 (1998).

[28]S. Succi, *The lattice Boltzmann equation for fluid dynamics and beyond* (Oxford University Press, Oxford, 2001).

[29]R. Zwanzig, *Nonequilibrium statistical mechanics* (Oxford University Press, New York, 2001).

[30]P. J. Dellar, "Bulk and shear viscosities in lattice Boltzmann equations," Phys. Rev. E **64**, 031203 (Aug 2001).

[31]D. Ricot, S. Marié, P. Sagaut, and C. Bailly, "Lattice Boltzmann method with selective viscosity filter," J. Comp. Phys. **228**, 4478–4490 (2009).

[32]M. M. Rogers and R. D. Moser, "Direct simulation of a self-similar turbulent mixing layer," Phys. Fluids **6**, 903–923 (1994).

[33]M. Terracol, P. Sagaut, and C. Basdevant, "A time self-adaptive multilevel algorithm for large-eddy simulation," J. Comp. Phys. **184**, 339–365 (2003).

[34]P. E. Dimotakis, "Turbulent free shear layer mixing and combustion," Progress in Astronautics and Aeronautics **137**, 265–340 (1991).